Electronic Supplementary Information

Mimicking Natural Photosynthesis: Sculpting Sunlight into Solar Fuel Via Sustained Photo-enzymatic Catalytic System Based on BT-NCOF Architecture

Anurag Rai,[a] Rajesh K. Yadav,*[a] Vitthal L. Gole,*[b] Kanchan Sharma,[a] Shaifali Mishra,[a] Rehana Shahin,[a] Jin Ook Baeg*[c]

[a]*Department of Chemistry and Environmental Science, Madan Mohan Malaviya University of Technology, Gorakhpur, 273010, (U.P.), India. *Email: rajeshkr_yadav2003@yahoo.co.in*

[b]*Department of Chemical Engineering, Madan Mohan Malaviya University of Technology, Gorakhpur, 273010, (U.P.), India.*

[c]*Korea Research Institute of Chemical Technology, 141 Gajeong-ro, Yuseong-gu, Daejeon, South Korea. *Email: jobaeg@krict.re.kr*

1. Material and Methods

Benzene-1,3,5-tricarbaldehyde (B), 4,4',4''-(benzene-1,3,5-triyltris(ethyne-2,1-diyl))trianiline (T), acetic acid, Triethanolamine (TEOA), N, N-dimethylformamide (DMF), tetrahydrofuran (THF), sodium phosphate dibasic dihydrate, sodium phosphate monobasic dihydrate, were purchased from Sigma-Aldrich and TCl Chemicals. The $[Cp^*Rh(bpy)\ (H_2O)]^{2+}$, i.e., Rh-C (Rhodium Complex mediator) was synthesised as per the reported paper.[1]

2. Instruments and Measurements

Fourier transform infrared spectroscopy (FTIR) were obtained using Shimadzu 8000 IR-spirit spectrometer. UV-Visible spectroscopy was recorded on Shimadzu UV-1900i spectrophotometer. Scanning electron microscope (SEM) images and elemental mapping were obtained on a Tescan Mira 3 LMU FEG SEM, Accelerating voltage: 10 kV, Coating: Quorum Q150T ES / 20 mA 60secPt coating. Cyclic Voltammetry, Tafel plot, Chronopotentiometry, EIS were performed on CHI608E, 220V instrument. TGA and DSC were performed using model: SDT Q600 V20.9 Build 20.

3. UV-visible spectroscopy of B and T and reflectance of BT-NCOF

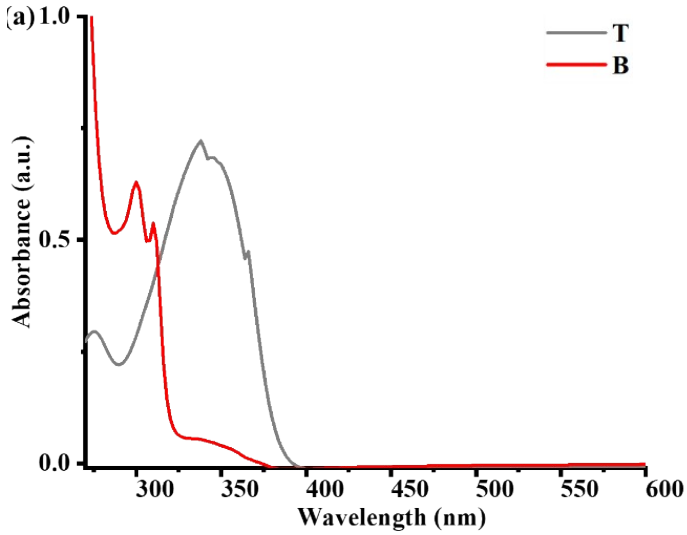

Figure S1. UV-visible spectroscopy of B, and T ($1*10^{-5}$ M in DMF).

4. Scanning electron microscopy (SEM) of B

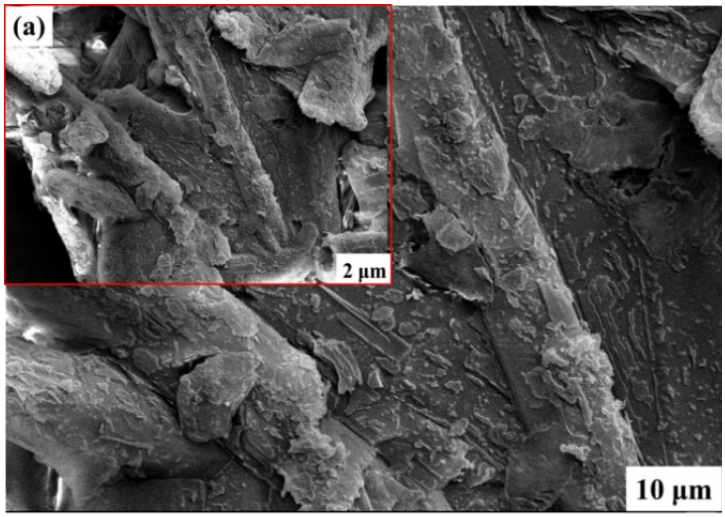

Figure S2. SEM images of B.

5. Comparison table for photocatalytic NADH regeneration

S.No.	Photocatalyst	e^- or H^- donor	Mediator	Temp.	Yield (%)	Ref.
1.	Ru@TiO2	Glycerol	Rh-C	25	1.25	[2]
2.	QD@F g-C3N4	TEOA	Rh-C	25	36	[3]
3.	g-C3N4	TEOA	Rh-C	25	56	[4]
4.	CCGCMAQSP	TEOA	Rh-C	25	45.5	[5]
5.	P-doped TiO2	H_2O	Rh-C	37	34.6	[6]
6.	BT-NCOF	TEOA	Rh-C	25	60.34	This Work

[@]**Reaction Condition:** Performed under inert atmosphere (N_2) in presence of solar light, where Rh-C work as an electron mediator between the photocatalyst and NAD^+.

Table S1. Photocatalytic regeneration of NADH via BT-NCOF photocatalyst.

The Comparative study shows the better photocatalytic activity of our synthesized BT-NCOF photocatalyst under solar light mediated reaction conditions. While other Ru@TiO_2 (1.25%), QD@F g-C_3N_4 (36%), g-C_3N_4 (56%), CCGCMAQSP (45.5%), QD@SiO_2 (70%), P-doped-TiO_2 (34.5%), shows low yield of NADH regeneration while the BT-NCOF photocatalyst shows better NADH regeneration yield as compared to other reported photocatalyst.

6. Tafel plots and linear fitting results along with EIS results for B, T and BT-NCOF

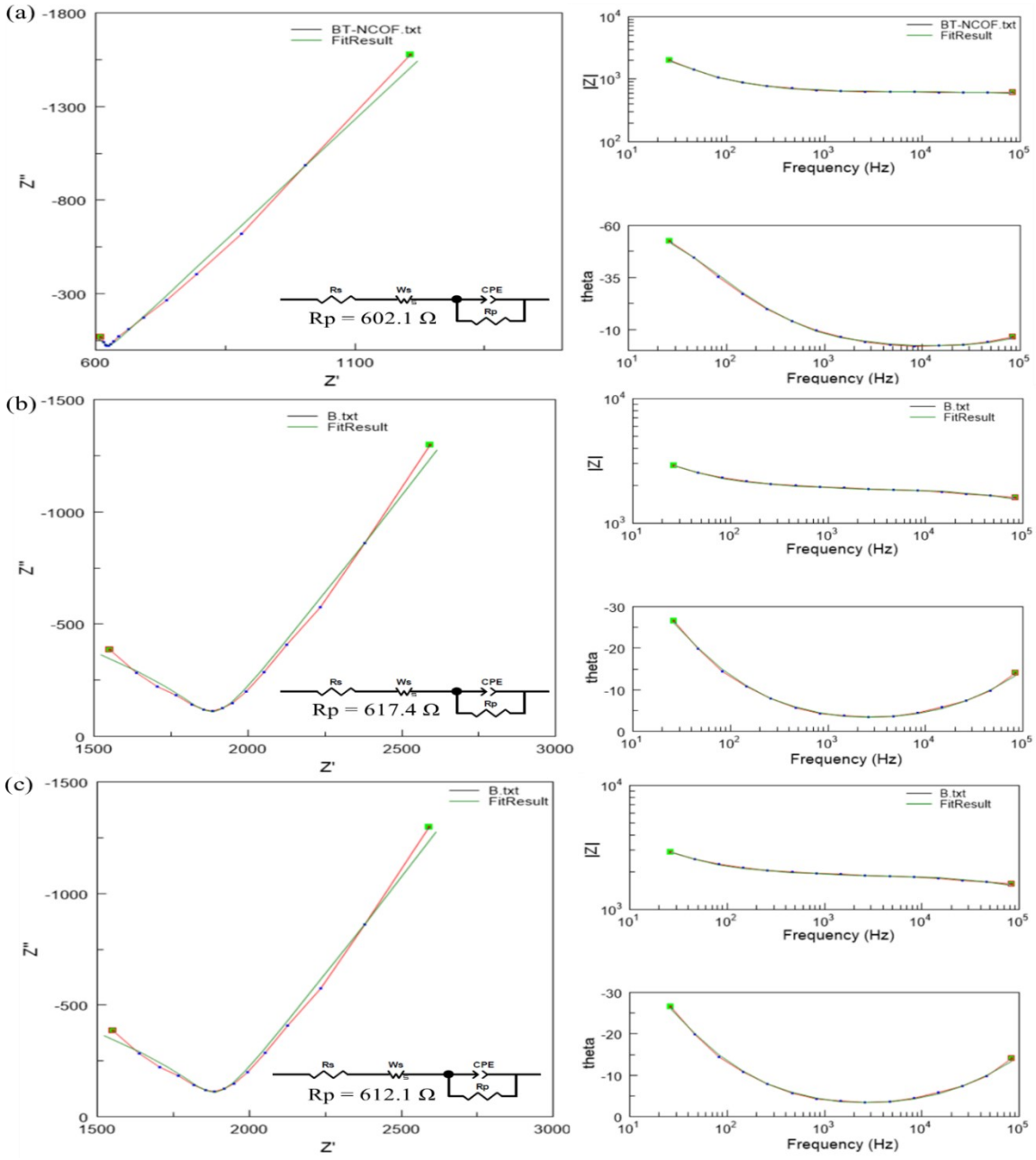

Figure S3: Nyquist plots (left), Bode magnitude and phase plots (right) of EIS spectra for (a) BT-NCOF, (b) T, and, (c) B. Experimental data are shown as scatter points and fitted curves obtained using Z-View software. Equivalent circuit models used for fitting are shown as insets, incorporating solution resistance (R_s), charge-transfer resistance (R_p), constant phase element (CPE), and Warburg diffusion element (W_o), capturing both interfacial and diffusion-related processes. The excellent fitting confirms the suitability of the circuit model in describing the electrochemical behavior of the BT-NCOF photocatalyst.

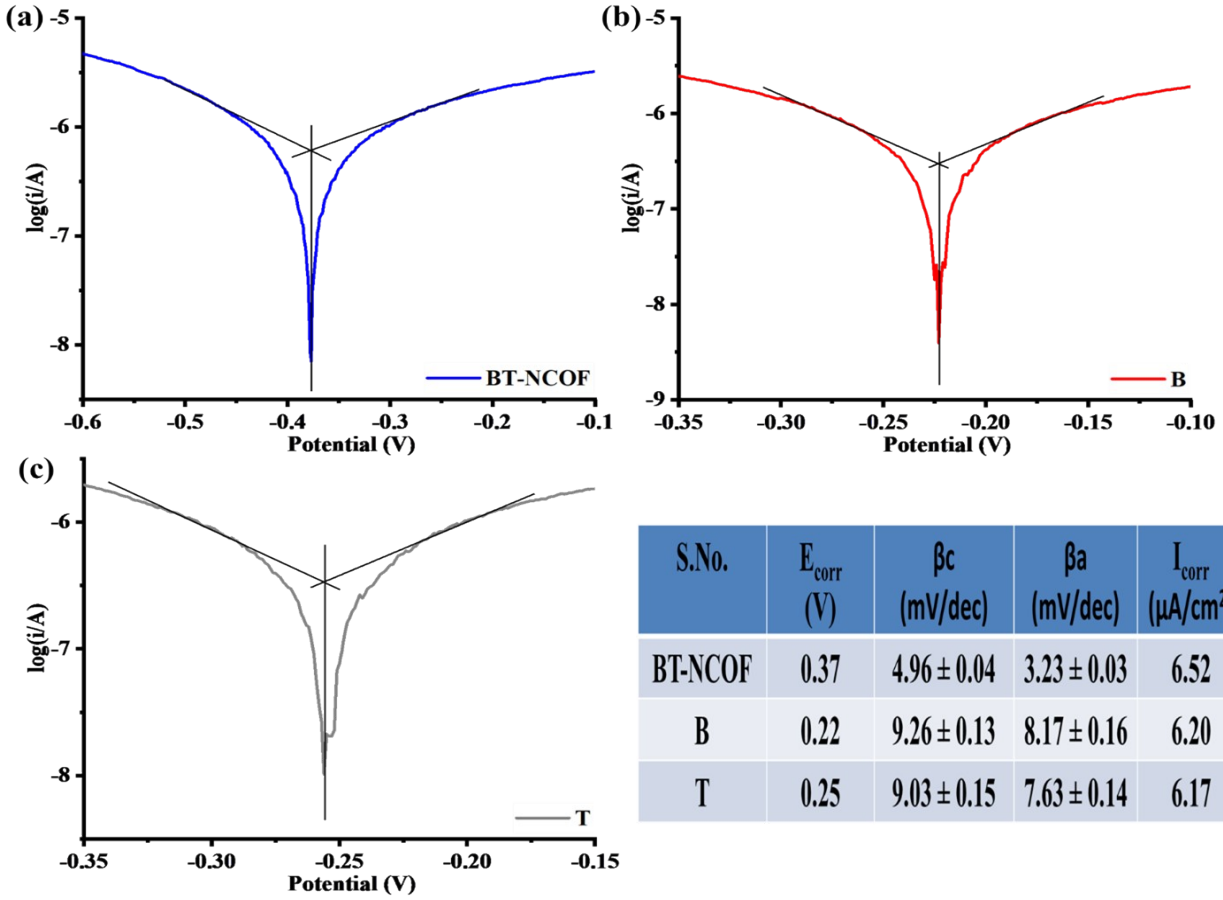

S.No.	E_{corr} (V)	βc (mV/dec)	βa (mV/dec)	I_{corr} (μA/cm²)
BT-NCOF	0.37	4.96 ± 0.04	3.23 ± 0.03	6.52
B	0.22	9.26 ± 0.13	8.17 ± 0.16	6.20
T	0.25	9.03 ± 0.15	7.63 ± 0.14	6.17

Figure S4: Tafel plots and linear fitting results for (a) BT-NCOF, (b) B, and (c) T. The experimental data are shown as plots with the fitted linear regions overlaid. Extracted Tafel slopes (both anodic (βa) and cathodic(βc)) and corrosion parameters (E_{corr}, I_{corr} for each material are summarized in the table, demonstrating the improved charge transfer kinetics of BT-NCOF.

7. Reusability and performance of BT-NCOF after multiple catalytic cycles

The reusability of the BT-NCOF for NADH and HCO_2H was evaluated by recovering the photocatalyst after each catalytic cycle through centrifugation method followed by washing. The recovered photocatalyst was then dried in an oven and reused for subsequent cycles. This procedure was repeated for five consecutive cycles to assess the stability and photocatalytic performance of the recycled catalyst. The results indicated that the yield remained stable, demonstrating good reusability. FTIR spectra were recorded before and after reaction performed, the ftir spectra peaks patterns exhibit similar characteristic peaks typical of BT-NCOF, indicating that its structure remains largely intact after repeated photocatalytic cycles. The absence of any significant shift in peak positions confirms that no major phase transformation occurred during the NADH regeneration and CO_2 fixation process. The spectra showed no significant changes in the characteristic peaks, confirming that the structural integrity of BT-NCOF was well preserved. Furthermore, the photocatalytic activity exhibited only minimal loss after repeated use, indicating that BT-NCOF retain their stability and functionality without noticeable degradation under prolonged irradiation.[7]

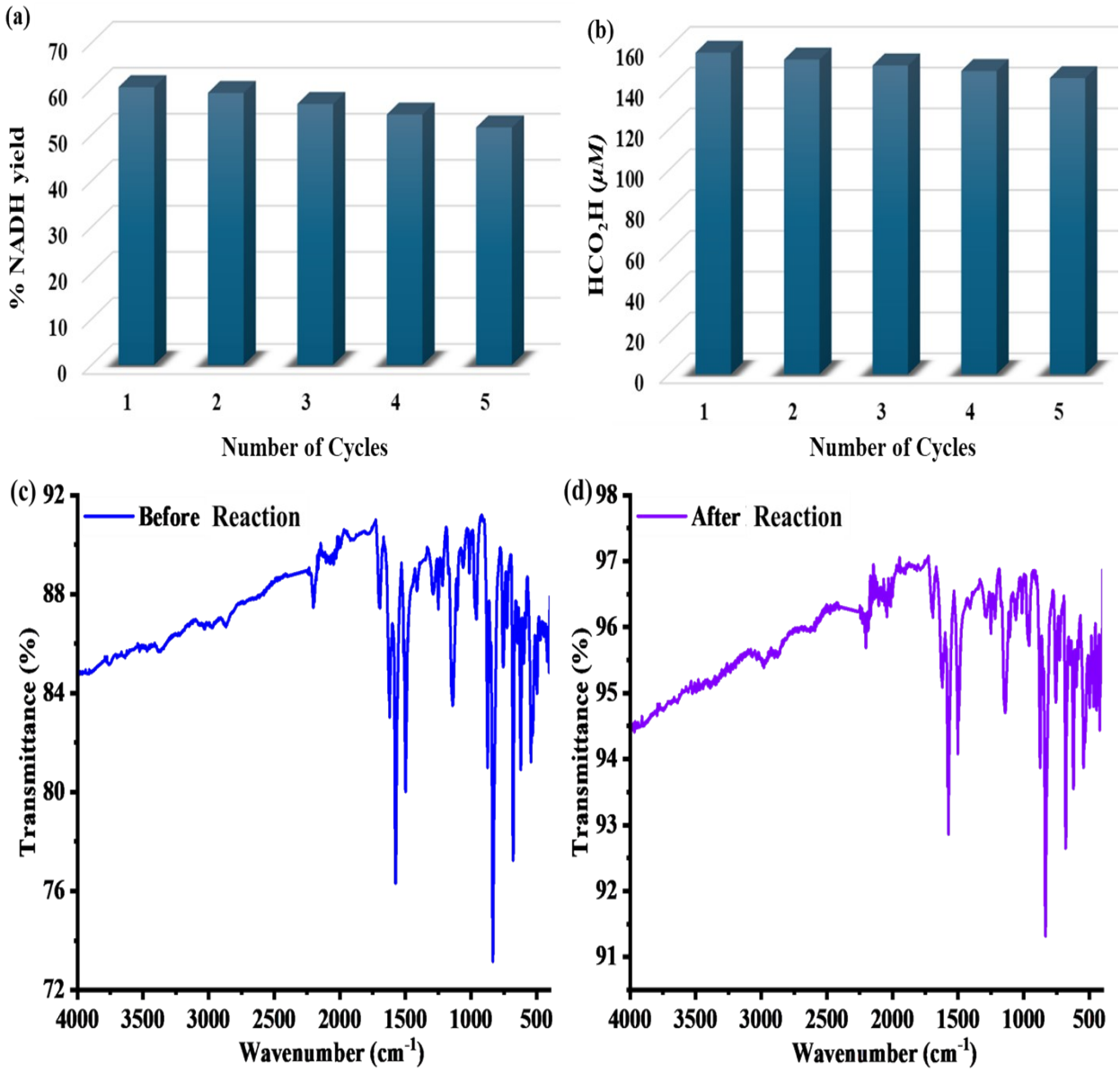

Figure S5: Recyclability performance of BT-NCOF photocatalyst up to five cycles (a) NADH regeneration, (b) conversion of CO_2 to HCO_2H, and FTIR spectra of BT-NCOF (c) before & (d) after the photocatalytic reaction. (@**Reaction Condition**: NAD^+ (248 µL), Rh-C mediator (124 µL), TEOA (310 µL) and photocatalyst (0.5 mg), FDH (3 units) in sodium phosphate buffer (100 mM, pH 7.0)).

8. Control experiments

To evaluate the CO_2 photoreduction and NADH performance via systematic control experiments conducted without photocatalyst, without FDH enzyme, without TEOA, and without light all produced no (almost zero) amounts of formic acid and NADH, confirming that each component is essential for the reaction (Figure S6). In addition, comparative studies using only precursor B as catalysts showed much lower activity than the BT-NCOF framework, demonstrating that the integrated structure is responsible for the enhanced performance (Table S2). These results, now included in the revised manuscript and Supporting Information, provide clear evidence that the observed NADH and formic acid yield arises from the intended photo–enzyme synergistic pathway rather than from any single factor alone.[7]

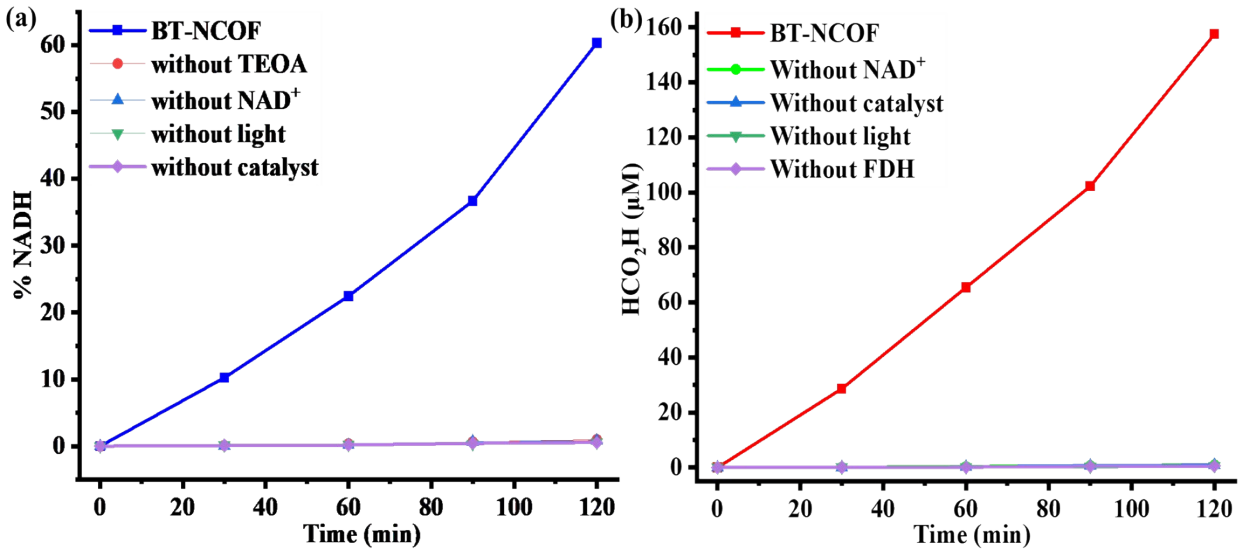

Figure S6: Control experiments for NADH regeneration and conversion of CO_2 to HCO_2H based on different reaction conditions. (@**Reaction Condition**: NAD^+ (248 μL), Rh-C mediator (124 μL), TEOA (310 μL) and photocatalyst (0.5 mg), FDH (3 units) in sodium phosphate buffer (100 mM, pH 7.0)).

Entry	Photocatalyst	Visible Light	Sacrificial Agent	Time (hr)	NADH Yield (%)	Formic Acid Yield (μM)
1.	B	-	TEOA	2	0	0
2.	B	+	-	2	0	0
3.	Absent	+	TEOA	2	0	0
4.	B	+	TEOA	2	4.71	15.7
5.	BT-NCOF	+	-	2	Trace	Trace
6.	Absent	+	TEOA	2	0	0
7.	BT-NCOF	+	TEOA	2	60.34	157.56

Table S2: Control experiment to evaluate the performance of NADH regeneration and CO_2 photoreduction. (@**Reaction Condition**: NAD^+ (248 μL), Rh-C mediator (124 μL), TEOA (310 μL) and photocatalyst (0.5 mg), FDH (3 units) in sodium phosphate buffer (100 mM, pH 7.0)).

9. PXRD of BT-NCOF

The PXRD spectra show main intense peaks at 2θ = 7.79° and 2θ = 9.88°; which correspond to the crystal planes of (100) and (110) for BT-NCOF. In addition, four weak peaks are observed at 2θ = 12.20°, 15.39°, 24.87° and 26.48°, which corresponds to (200), (210), (301) and (001) planes, respectively (Figure S8). Remarkably the comparison of experimental PXRD patterns with the simulated profile demonstrates a good agreement, confirming the formation of a hexagonal COF structure generated via coupling between benzene-1,3,5-tricarbaldehyde (B) and multi-amine linkers (4,4',4"-(benzene-1,3,5-triyltris(ethyne-2,1-diyl))trianiline (T)).

Calculation of crystalline size: -

$$\mathbf{D} = \frac{K\lambda}{\beta Cos\Theta}$$

Where,

D = crystalline size (nm)

K = 0.9 (Scherrer constant)

λ = 0.15406 nm (wavelength of the x-ray sources)

β = FWHM (radians)

Θ = Peak position

S.No.	2Θ (Peak position)	β (FWHM)	Crystalline Size (D)	Avg. Crystalline Size (D)
1.	7.79349	0.66761	12.01053	**28.89 nm**
2.	9.88884	0.43041	18.73585	
3.	12.20177	0.29264	27.77441	
4.	15.39202	0.1941	42.45148	
5.	24.87324	0.20726	42.24906	
6.	26.48345	0.29428	30.16064	

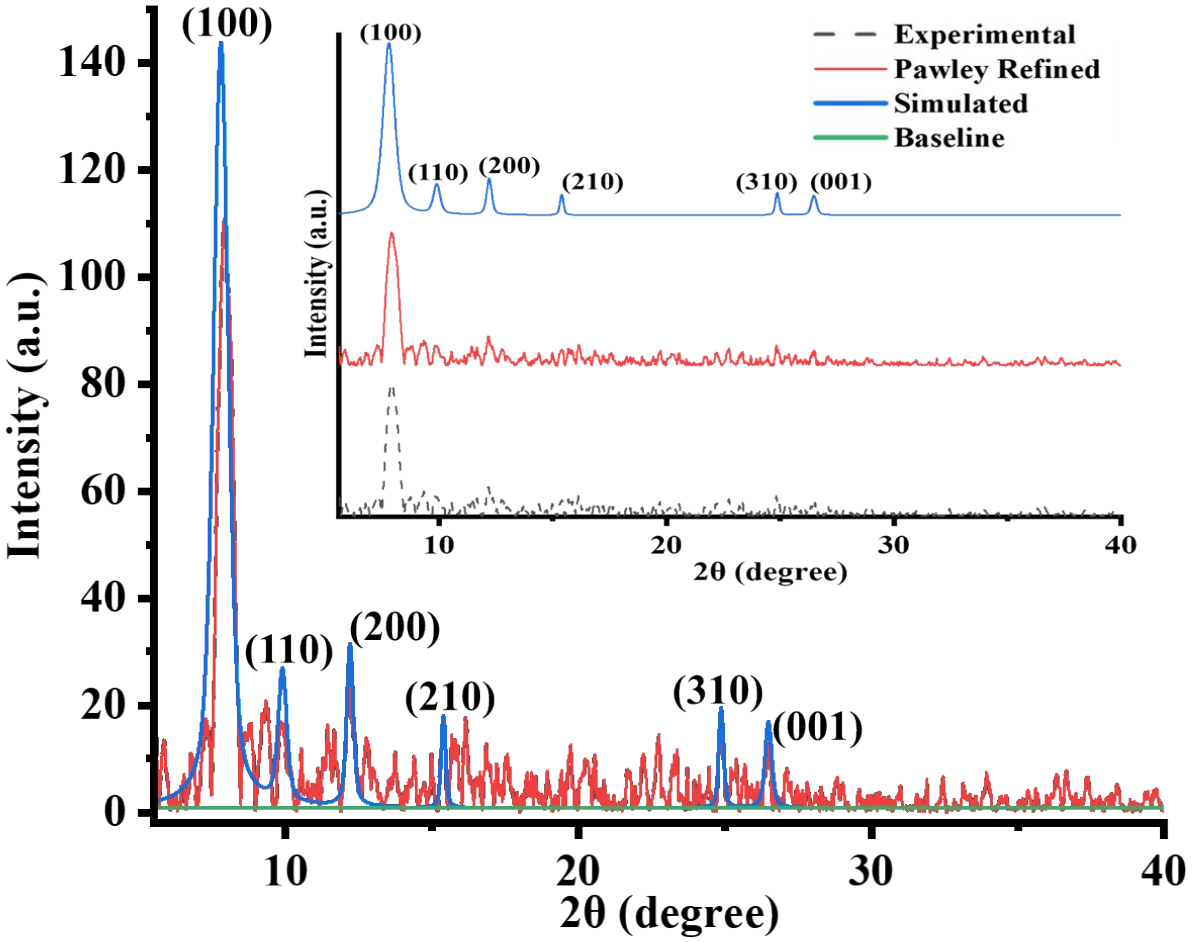

Figure S7: PXRD of BT-NCOF photocatalyst along with experimental, baseline, refined, and simulated pattern (inset scattered form).

10. Reactive oxygen species trapping (ROS)

Reactive oxygen species trapping experiments was performed to capture the active species during the photocatalytic process to verify the possible charge transfer pathways. During the photocatalytic experiments the isopropanol (IPA), ethylenediaminetetraacetic acid disodium salt (EDTA-2Na), L-ascorbic acid, and $AgNO_3$ were used as capture agents for e^-, •OH, $•O_2^-$and h^+, respectively. The photocatalytic control experiments were performed using the capture agents to monitor the difference in NADH yield, as the capture of e^- will hinder the NADH regeneration, confirming the dominant effect of e^- in the charge transfer from photocatalysts to NAD^+. The introduction of capture agents IPA and L-ascorbic acid during the photocatalytic regeneration of NADH didn't cause much yield loss in the process, indicating that only a small amount of •OH and $•O_2^-$ were produced during NADH regeneration. However, the capture agent consumed free radicals and promoted the participation of e^- in free radical production, the amount of e^- involved in NAD^+ reduction was reduced and the activity was slightly lowered. When EDTA-2Na was introduced in the reaction system, the system already had TEOA as a h^+ sacrificial agent. The addition of EDTA-2Na caused an excess of sacrificial agent, which decomposed the already produced NADH and therefore the yield of NADH decreased at last. $AgNO_3$ hinders NADH regeneration as its addition leads to reduced NADH yield. $AgNO_3$ acts as an inhibitor to the enzymatic pathways necessary for NADH regeneration because silver ions are highly reactive which disrupt the NADH regeneration (Figure S8).[8]

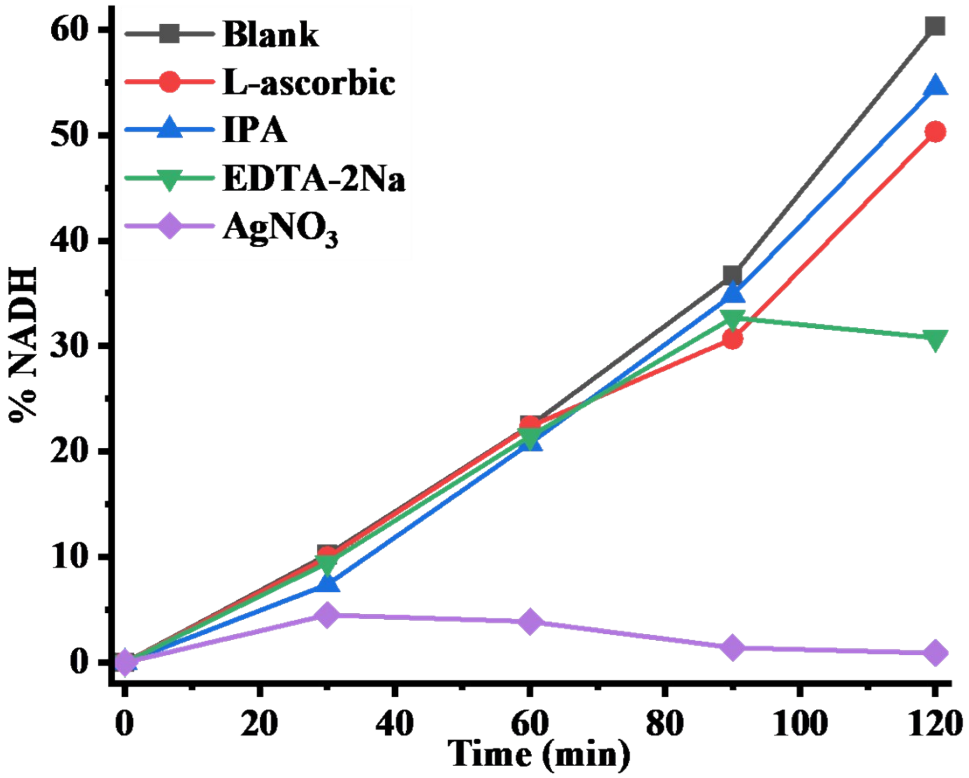

Figure S8. Control experiments were performed by using capture agents for NAD^+.

References

1 P. Haquette, B. Talbi, L. Barilleau, N. Madern, C. Fosse and M. Salmain, *Org. Biomol. Chem.*, 2011, **9**, 5720–5727.

2 M. Aresta, A. Dibenedetto, T. Baran, A. Angelini, P. Łabuz and W. Macyk, *Beilstein J. Org. Chem.*, 2014, **10**, 2556–2565.

3 D. Yang, H. Zou, Y. Wu, J. Shi, S. Zhang, X. Wang, P. Han, Z. Tong and Z. Jiang, *Ind. Eng. Chem. Res.*, 2017, **56**, 6247–6255.

4 X. Huang, J. Liu, Q. Yang, Y. Liu, Y. Zhu, T. Li, Y. H. Tsang and X. Zhang, *RSC Adv.*, 2016, **6**, 101974–101980.

5 G. Centi, S. Perathoner, C. Genovese and R. Arrigo, *Chem. Commun.*, 2023, **59**, 3005–3023.

6 Q. Shi, D. Yang, Z. Jiang and J. Li, *J. Mol. Catal. B Enzym.*, 2006, **43**, 44–48.

7 S. Singh, S. Y. Choi, R. K. Yadav, C. Y. Na, J. Kim, M. Y. Choi and T. W. Kim, *Energy & Fuels*, 2025, **39**, 1746–1758.

8 Y. Zhou, Y. He, M. Gao, N. Ding, J. Lei and Y. Zhou, .